High-Coulombic-Efficiency Carbon/Li Clusters Composite Anode without Precycling or Prelithiation

Ran Tian, Huanan Duan,* Yiping Guo, Hua Li, and Hezhou Liu*

Lithium metal has attracted much research interest as a possible anode material for high-energy-density lithium-ion batteries in recent years. However, its practical use is severely limited by uncontrollable deposition, volume expansion, and dendrite formation. Here, a metastable state of Li, Li cluster, that forms between LiC_6 and Li dendrites when over-lithiating carbon cloth (CC) is discovered. The Li clusters with sizes in the micrometer and submicrometer scale own outstanding electrochemical reversibility between Li^+ and Li, allowing the CC/Li clusters composite anode to demonstrate a high first-cycle coulombic efficiency (CE) of 94.5% ± 1.0% and a stable CE of 99.9% for 160 cycles, which is exceptional for a carbon/lithium composite anode. The CC/Li clusters composite anode shows a high capacity of 3 mAh cm^{-2} contributed by both Li^+ intercalation and Li-cluster formation, and excellent cycling stability with a signature sloping voltage profile. Furthermore, the CC/Li clusters composite anode can be assembled into full cells without precycling or prelithiation. The full cells containing bare CC as the anode and excessive $LiCoO_2$ as the cathode exhibit high specific capacity and good cyclic stability in 200 cycles, stressing the advantage of controlled formation of Li clusters.

Nowadays, the energy and environment issues promote the development of the power devices. Li-ion batteries (LIBs), as the most widely used energy storage devices, have attracted the attention of the researchers to enhance the energy density and working life.[1] Lithium metal, due to its advantages in light weight (0.53 g cm^{-3}), the lowest electrochemical potential (−3.04 V vs the standard hydrogen electrode), and high theoretical specific capacity (3840 mAh g^{-1}), has been regarded as an ideal anode for LIBs.[2] But there are still some issues. The biggest issue, Li dendrite formation, is caused by the cracks formed in the solid–electrolyte interphase (SEI) layer between Li and electrolyte as a result of the drastic volume change during continuous Li stripping/plating and hard to be solved.[3]

In recent years, some useful electrolyte progresses such as optimizing the solvents,[4] lithium salts,[5] electrolyte additives;[6] introducing high-modulus solid electrolytes (such as LLZO,[7]

R. Tian, Prof. H. Duan, Prof. Y. Guo, Prof. H. Li, Prof. H. Liu
State Key Laboratory of Metal Matrix Composites
School of Materials Science and Engineering
Shanghai Jiao Tong University
Shanghai 200240, P. R. China
E-mail: hd1@sjtu.edu.cn; hzhliu@sjtu.edu.cn

The ORCID identification number(s) for the author(s) of this article can be found under https://doi.org/10.1002/smll.201802226.

PEO,[8] LiPON[9]) have been developed to enhance the electrochemical performance of the Li metal anode. But these methods do not change the essence of the Li metal anode and need excessive Li to compensate the consumption of the Li element due to the formation the unstable SEI layer and dead Li.[10] The excessive Li can hardly realize the ultimately high power density and often causes safety issues in the charge and discharge process.[2b]

To improve the property of the Li metal anode, a substrate method—growth of Lithium on a suitable substrate has been proposed. In particular, the substrates with 3D conductive network and lithiophilic property have shown stable Li metal deposition behavior during the plating/stripping process.[2a] The substrates mainly contain graphene,[11] carbon nanotubes,[12] graphene nanoribbons,[13] 3D Cu network,[14] metal oxides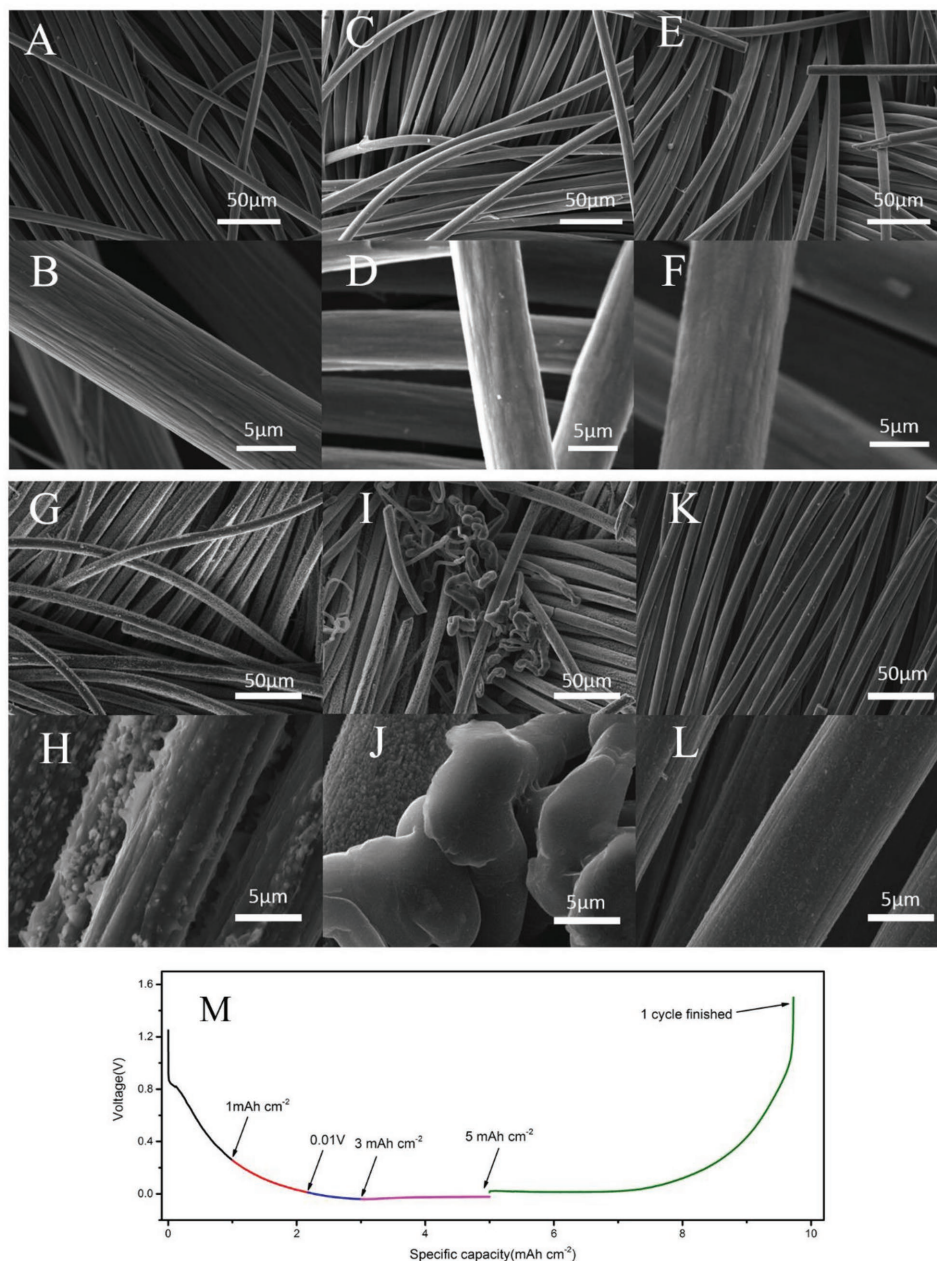/carbon composites,[15] and so on. Among these, the carbon-based materials with various material properties such as different morphology and structures, heteroatom doping, and surface modification have been investigated to improve Li metal deposition. For example, Zhang and his co-workers found that nitrogen (N)-doped graphene could change the Li metal nucleation and suppress Li-dendrite growth.[16] Therefore, the Li metal deposited on the N-doped graphene substrate shows dendrite-free morphology during the charge/discharge process and exhibits a coulombic efficiency (CE) of 98% for 200 cycles. Herein, CE is one of the most important parameters for the high-capacity substrate-based anode because the substrates are Li-ion free and the Li-ion supply from cathode is rather limited in practical Li-ion cells. However, so far there is little research about lithium anode where CE could reach the commercial graphite standard (CE > 90% in the first cycle and CE > 99.8% thereafter). It is suggested that the substrates should be precycled or prelithiated before assembling the full cell to obtain a high specific capacity.[14a,15a,17]

In a previous work, the excessive charging in the LIBs can form Li dendrites on the anode, which affects the capacity and give rise to safe issues.[18] To analyze the Li-dendrite-formation process on common carboneous materials, we used commercial carbon cloth as the substrate. Both D and G bands in the Raman spectrum (Figure S1A, Supporting Information) and broad peaks in the X-ray diffraction (XRD) data (Figure S1B, Supporting Information) suggest that the carbon cloth has a hybrid texture of layer-structured graphite and unorganized

**ADVANCED
SCIENCE NEWS**
www.advancedsciencenews.com

NANO · MICRO
small
www.small-journal.com

Figure 1. Characterizations of CC electrodes upon Li-metal deposition. A–L) SEM images of A,B) a bare CC electrode and the electrode lithiated to C,D) 1 mAh cm^{-2}, E,F) 0.01 V G,H) 3 mAh cm^{-2}, and I,J) 5 mAh cm^{-2}. K,L) SEM images of the electrode after 1 cycle. M) Voltage–capacity profile of the whole process.

carbon.[19] In consequence, the Li deposition process of a more disordered carbon can be characterized into two processes, e.g., the intercalation into the layer structure and the insertion into the unorganized carbon. Also the discharge voltage profile of the carbon cloth does not have obvious voltage platforms associated with the formation of staged phases as the graphite.[18,20]

To analyze the Li metal deposition process, we took the Li/carbon cloth (CC) cell to proceed a galvanostatic discharge/charge (intercalation/deintercalation) for one cycle at 0.2 mA cm^{-2}. From the scanning electron microscopy (SEM) images of CC (**Figure 1**A,B), the fiber diameter is about 10 µm with a smooth

surface. After discharging to 1 mAh cm^{-2} (Figure 1C,D) and 0.01 V (about 2.1 mAh cm^{-2}, Figure 1E,F), the appearance of CC does not have distinct change, which implies that the main electrochemical reaction is the insertion of Li ion into the carbon cloth to form Li$_x$C$_6$.[21] When the discharge (intercalation) proceeds to 3 mAh cm^{-2} (Figure 1G,H), Li clusters with the size of about 1 µm show up on the CC fiber surface, which indicates that the CC has been over-lithiated. The clusters are the seed crystals for dendrite growth which take shape below 0 V versus Li$^+$/Li and form a composite with the CC.[18] It is important to mention that till this point, the voltage exhibits a gradual and

ADVANCED
SCIENCE NEWS
www.advancedsciencenews.com

NANO · MICRO
small
www.small-journal.com
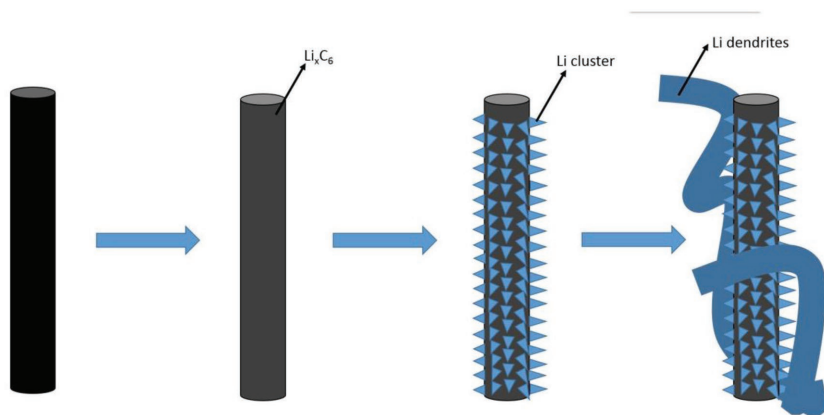
Scheme 1. Schematic presentation of the lithiation process of a carbon fiber.

slow decay (Figure 1M), implying the mixed texture of CC and the ongoing increase of the surface concentration of intercalated Li.[22] After discharging to 5 mAh cm−2, the voltage is then determined by Li plating and shows a plateau (Figure 1M). Indeed, the SEM images (Figure 1I,J) show that Li dendrites appear in the interspace of the carbon fibers. Besides, the Li clusters still retain and bestrew the fiber surface. Finally, when the CC is charged (deintercalated) back to 1.5 V, the CC almost turns to its original appearance except that the fiber surface looks a little rough as a result of the SEI formation (Figure 1K,L). Similarly, side-view SEM images of the electrode (Figure S2, Supporting Information) show that the formed Li clusters surround the carbon fiber after discharging to 3 mAh cm−2. When reaching 5 mAh cm2, the fibers are connected by the Li metal. The whole over-lithiation process can be described as the **Scheme 1**. Li ions first insert and/or intercalate into the CC to form Li_xC_6; then the Li clusters and Li dendrites form on the CC surface depending on the over-lithiation depth.

We further carried out the galvanostatic cycling tests at 1 mA cm−2 from 1.5 V to 3 or 5 mAh cm−2 for the Li/CC cells (denoted as Li/CC 3 mAh cm−2 cell and Li/CC 5 mAh cm−2 cell, respectively) to study the effect of deposition depth on the CE.[23] As shown in **Figure 2**A, the Li/CC 3 mAh cm−2 cell exhibits CE of 94.2% in the first cycle due to the irreversible SEI layer formation. By collecting the first CE data from another five cells, we received the first CE of Li/CC 3 mAh cm−2 cell is 94.5% ± 1.0%. After the first several cycles, the CE quickly increases to 99.5% and maintains around 99.9% without any significant drop in the following 160 cycles. The voltage-capacity curves for different cycles (Figure S3A, Supporting Information) show that the voltage profiles almost coincide for cycle 10, 50, and 100. In contrast, the Li/CC 5 mAh cm−2 cell gives slightly lower CE in the first 30 cycles than the Li/CC 3 mAh cm−2 cell. But after 30 cycles, serious CE drop to 90% occurs, suggesting that the specific capacity of 5 mAh cm−2 is not suitable for the CC anode.[24] In the voltage-capacity curves (Figure S3D, Supporting Information), the decrease of the charge capacity appears due to the dead-Li formation. As a comparison, bare Cu foil shows very unstable CE and huge polarization (Figure S4, Supporting Information) because the interfacial incompatibility between Cu and Li metal causes severe dead-Li formation.[14c,25] We also test the CE of the Li/CC 3 mAh cm−2 cells at current densities

of 3, 6 mA cm−2 in ether-based electrolyte and 3 mAh cm−2 cells at current densities of 1 mA cm−2 in the esters-based electrolyte. Again, the steadily high CE (Figure S5, Supporting Information), well-matched voltage-capacity curves in different cycles (Figure S3B,C, Supporting Information) and very similar cluster morphology (Figure S6, Supporting Information) demonstrate excellent reversibility of the Li clusters, which is very suitable for commercial use. Nevertheless, the Li/CC 3 mAh cm−2 cells at high current density cannot reach high cycle numbers, probably because of the unstable deposition/stripping process of the Li metal counter electrode and the subsequent short circuit.

Afterwards, we studied the reasons why different deposition capacities cause the different electrochemical performance. SEM images of the Li/CC 5 mAh cm−2 cell after 50 cycles (Figure S7, Supporting Information) clearly show large amount of dead Li forms on the top of the CC electrode with loose attachment to the conductive carbon networks. The dead Li leads to low CE and may cause safety issues.[2a] On the other hand, the Li/CC 3 mAh cm−2 cells after 50 cycles (Figure S8, Supporting Information) have very similar morphology compared to those in the first cycle (Figure 1G,H). Specifically, Figure S8A,B in the Supporting Information reveals that dense Li clusters covered on the CC electrode surface after the 50th discharge without the formation of Li dendrites or dead Li. To further study the distribution and properties of Li element in different forms of plated Li such as Li clusters and the Li dendrites, time-of-flight (TOF)-secondary ion mass spectrometry (SIMS)-SEM analysis was taken. The electrodes with Li clusters or Li dendrites were prebeamed by Gallium ions to wipe off the influence of the SEI layer. From Figure 2B–G, we can observe a few interesting points between the Li clusters and Li dendrites. First, the weak ^{19}F mapping (Figure 2D,G) implies that the SEI layer has been almost completely removed by prebeaming. Second, Figure 2C confirms that the fiber surface is covered by dense Li clusters. Third, it is intriguing that, as displayed in Figure 2F, Li elements in the form of Li_xC_6 and Li clusters have stronger signal than those in the form of Li dendrites, which is consistently observed in different samples with dendrite formation. It is well known that in TOF-SIMS, the brighter is the image, the larger is the number of secondary ion counts recorded at the corresponding mass fragment. Thus, we speculate that the strong Li signals can only be due to that the Li in Li_xC_6 and the cluster-form Li are more active under Gallium ion sputtering and easier to transfer into secondary Li^+ than those in the dendrites. This also suggests that the metallic Li in the clusters may have high activity and easily transform to Li^+ with energy sources such as ion beam and electrochemical potential. As a result, we believe that when the CC electrode is discharged below 0.01 V versus Li/Li^+ to 3 mAh cm−2 in Figure 1M, the formations of Li_xC_6 and Li clusters are symbiotic and there is no obviously voltage plateau. On the contrary, the Li dendrites show much weaker signals than the fibers in the [7]Li mapping. This phenomenon indicates that the metallic Li in dendrites mainly formed at the voltage platform below 0 V

ADVANCED
SCIENCE NEWS
www.advancedsciencenews.com

NANO · MICRO
small
www.small-journal.com
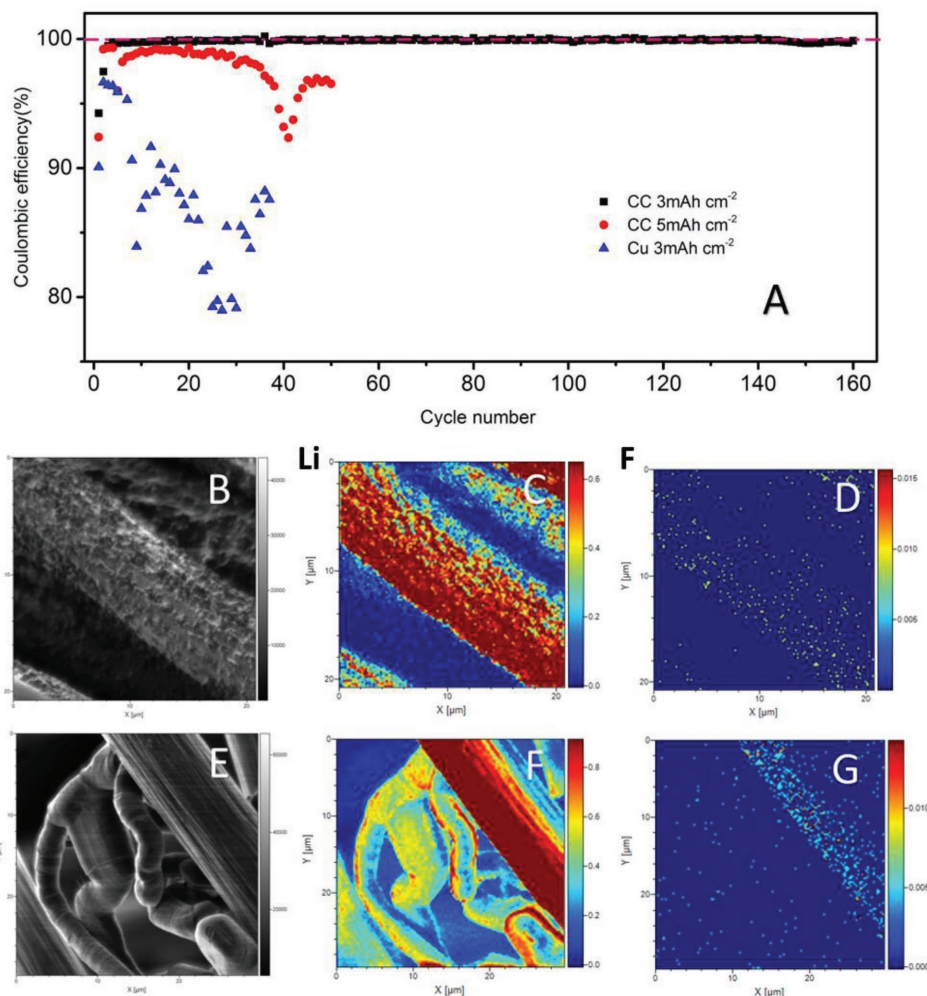
Figure 2. Characterizations of CC/Li-metal composite anodes. A) Coulombic efficiencies of different electrodes at the current density of 1 mA cm^{-2}. B, E) The TOF-SEM, C,F) ^{7}Li TOF-SIMS mapping and D,G) ^{19}F TOF-SIMS mapping of the CC/Li clusters composite anode discharged to 3 and 5 mAh cm^{-2}, respectively.

versus Li/Li$^+$ is relatively inactive. The highly active Li clusters have the electrochemical property analogous to the Li$_x$C$_6$ so that the Li/CC 3 mAh cm^{-2} cell can have ultrahigh CE like graphite anode.

To further evaluate the electrochemical performance of the CC/Li clusters composite anode, more galvanostatic cycling was employed. Herein, the Li/CC cells were first discharged to 5 and 3 mAh cm^{-2}, respectively, and then were cycled at 1 mA cm^{-2} to 1 mAh cm^{-2} for 100 cycles. The voltage–time profiles (**Figure 3**A) of Li/CC 5 mAh cm^{-2} show flat platform without throb. By examining the corresponding SEM images (Figure 3C,D), Li metal with flake structure grows on the CC surface on the side against the Li counter electrode. The surface of fiber turns to the smooth morphology due to the transformation from the Li clusters to massive Li metal. On the other hand, the Li clusters are the metastable state with high activity and the Li dendrites are the stable state. The high CE of the Li/CC 3 mAh cm^{-2} cell is contributed by the highly active and small Li clusters. In addition, the property of the Li/CC 3 mAh cm^{-2} cell was measured as the same means with the

Li/CC 5 mAh cm^{-2} cell. (Figure 3B). It is seen that there is no pleatue but the diagonal in the time–voltage picture. It demonstrated that the Li clusters do not have the tendency to form Li dendrites during the cycling process near 0 V versus Li$^+$/Li. Compared with the specific capacity of CC at the range of 0.01–3 V (Figure S9, Supporting Information), the 3 mAh cm^{-2} is immensely higher than the origin capacity. Quantitatively, the calculation of the specific capacity of the whole electrode of CC and graphite (Content S1, Supporting Information) shows that the CC electrode with 3 mAh cm^{-2} has about 57.2% enhancement compared with the graphite electrode. This considerable improvement means that the CC/Li-clusters composite anode may find practical applications in high-energy LIBs.
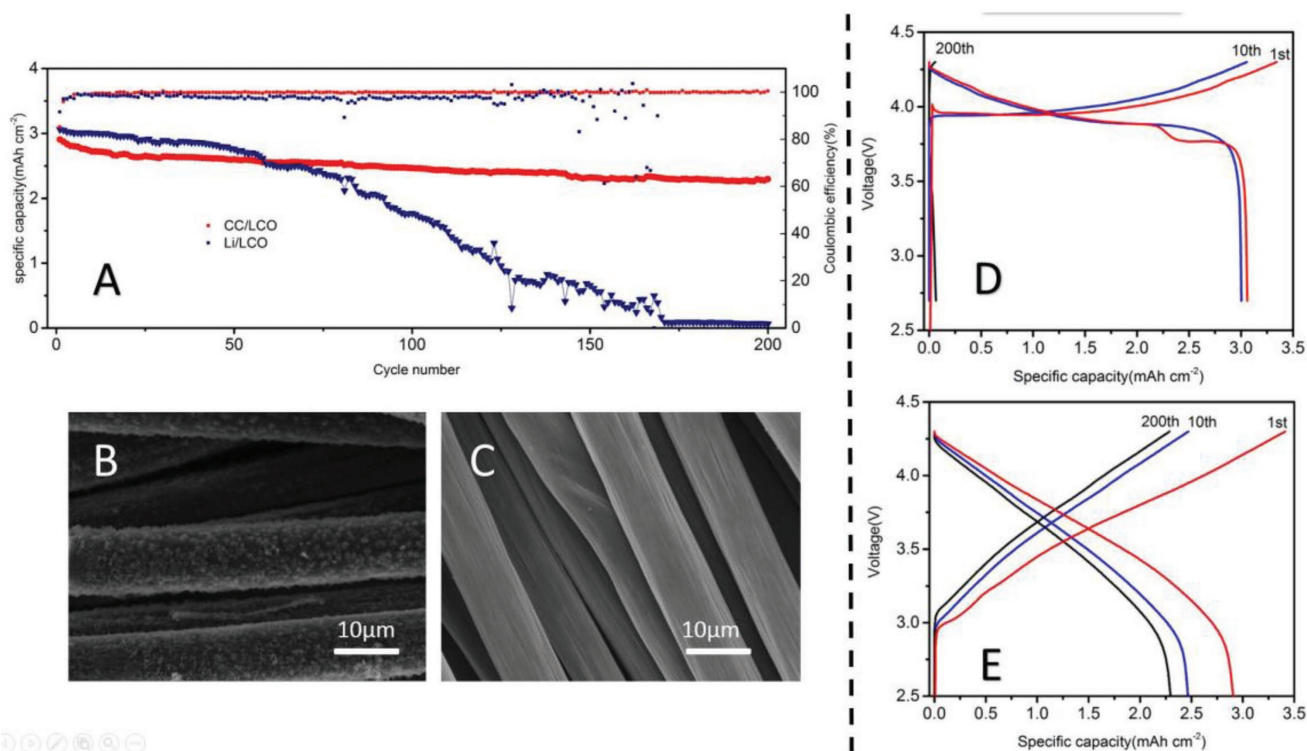
Figure S10 in the Supporting Information shows the X-ray photoelectron spectroscopic (XPS) data of the CC electrodes of the Li/CC 3 mAh cm^{-2} cells and Li/CC 5 mAh cm^{-2} cells. In the C 1s high-resolution spectra, the three peaks correspond to C—C or LiC$_6$, C—O—C, and CO$_3$$^{2-}$. The CO$_3$$^{2-}$ mainly comes from the reaction of between Li metal and air during the transport process. Obviously in Figure S10A,B in the Supporting

**ADVANCED
SCIENCE NEWS**
www.advancedsciencenews.com

NANO · MICRO
small
www.small-journal.com
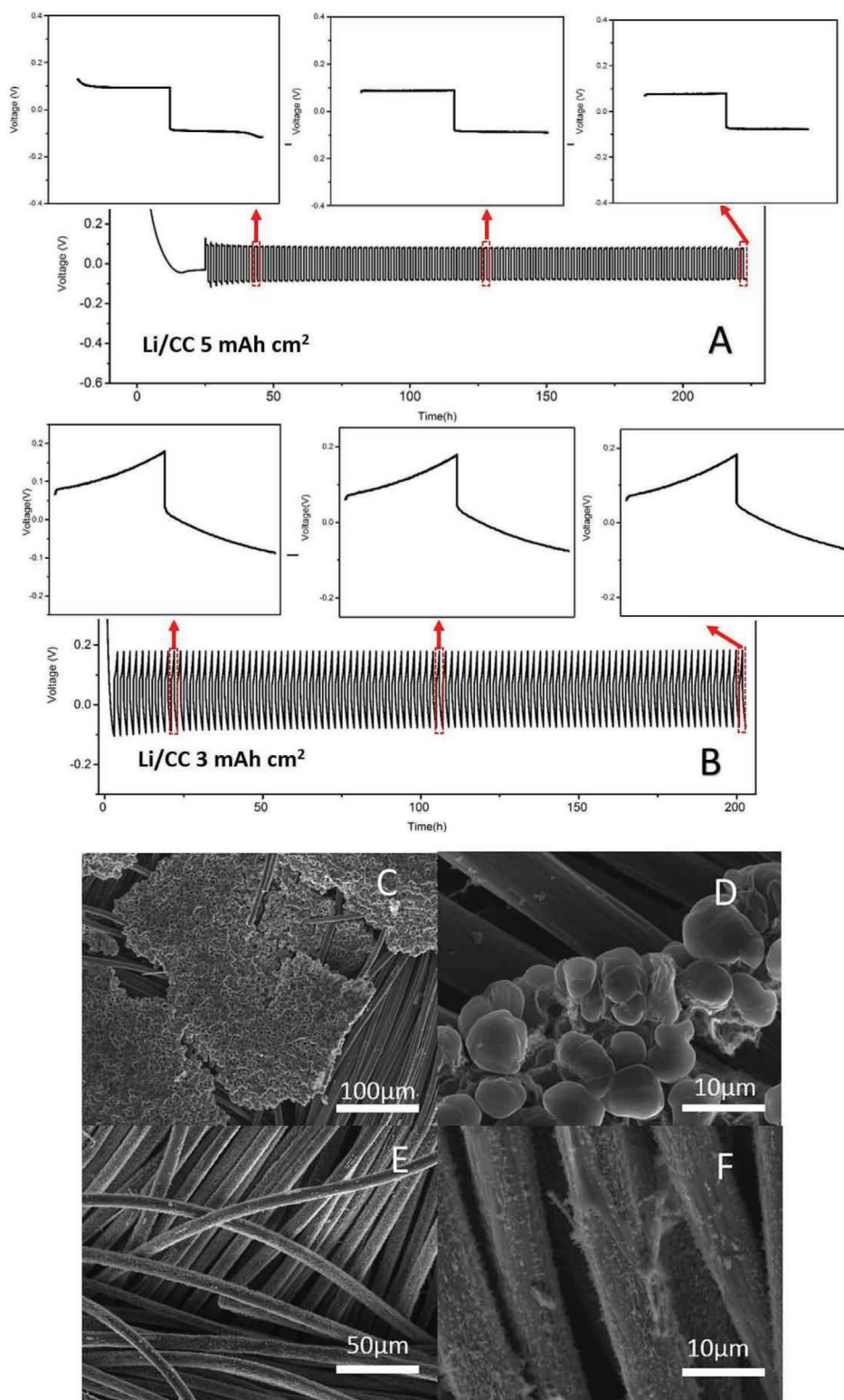
Figure 3. Performance of the Li/CC 3 mAh cm^{-2} cell and Li/CC 5 mAh cm^{-2} cell cycled at 1 mA cm^{-2} to 1 mAh cm^{-2}. Voltage–time curves of A) the Li/CC 5 mAh cm^{-2} cells and B) the Li/CC 3 mAh cm^{-2} cells. Insets, expanded view of the corresponding voltage profiles. SEM images of the CC electrodes in C,D) the Li/CC 5 mAh cm^{-2} cells and E,F) the Li/CC 3 mAh cm^{-2} cells after 100 cycles.

Information, the content of the CO_3^{2-} in the Li/CC 5 mAh cm^{-2} cell is higher than that in the Li/CC 3 mAh cm^{-2} cell, indicating higher amount of plated Li metal in the CC. Besides, it confirms the presence of Li clusters by the significant amount CO_3^{2-} in the Li/CC 3 mAh cm^{-2} cell. The Li 1s spectra (Figure S12C,D, Supporting Information) is consistent with the

ADVANCED
SCIENCE NEWS
www.advancedsciencenews.com

NANO · MICRO
small
www.small-journal.com

Figure 4. Performance of the Li/LCO and CC/LCO full cells. A) Capacity retention and CE of the cells cycled at 0.6 mA cm^{-2}. SEM images of the CC electrode after the first B) charge and C) discharge process. Voltage–capacity profiles of different cycles for D) Li/LCO and E) CC/LCO cells.

C 1s spectra above, i.e., the peak of the Li—CO$_3$ bond in the Li/CC 5 mAh cm^{-2} sample is much higher than that in the Li/CC 3 mAh cm^{-2} cell.

It is well-known that the cells using Li metal anode usually contain excessive Li to maintain stable cycling performance. As a result, it cannot really boost the energy density. On the other hand, the substrate method for full-cell use often requires precycling or prelithiation process to enhance the specific capacity (more discussion is in Content S2 in the Supporting Information).[14a] In this work, we constructed CC/LCO (LiCoO$_2$) cells to evaluate the full-cell property by taking advantage of the excellent electrochemical property of the Li clusters. To match the 3 mAh cm^{-2} on the CC anode side, a commercial LiCoO$_2$ cathode with an areal loading mass of about 18.9 mg cm^{-2} on aluminum foil (Figure S11, Supporting Information) was employed. An ester-based electrolyte was used to attain a test voltage range of 2.5–4.3 V. **Figure** 4A shows the cyclic performance of CC/LCO and Li/LCO cells at a current density of 0.6 mA cm^{-2} (about 0.2 C). In the first cycle, the Li/LCO cell has a specific charge capacity of 3.34 mAh cm^{-2} and a specific discharge capacity of 3.06 mAh cm^{-2}, corresponding to a CE of 91.6 %. The cell shows relatively stable performance in the first 50 cycles and then encounters an evident CE decrease with a slow capacity drop. After the 110th cycle, enormous capacity fluctuation appears and sustains until short circuit occurs and the capacity turns to be closed to 0 mAh cm^{-2}. This phenomenon is common in the cell with Li metal anode due to the unstable SEI layer and the formation of mossy Li and dead Li. On the contrary, the CC/LCO cell exhibits long and stable cyclic performance. The specific charge and discharge capacity

are 3.41 and 2.91 mAh cm^{-2}, respectively, in the first cycle, corresponding to a CE of 85.2%, which is a little lower than that of the Li/LCO cell. This slightly lower CE is due to the fact that some of Li element is consumed during the SEI layer formation in the first cycle. Morphology study in Figure 4B,C clearly shows that the Li clusters grow on the carbon fibers and then vanish after the first whole cycle. After the first several cycles, the CE quickly increases to 99.5% and maintain around 99.8%. After the 59th cycle, the CC/LCO cell surpasses the Li/LCO cell in terms of the specific capacity, eliminating the capacity loss from the SEI formation in the first cycle. After the 200th cycle, the CC/LCO cell still owns a capacity of 2.30 mAh cm^{-2}, which is 79% of the initial capacity. It is remarkable that during the whole cycling process, no capacity fluctuation is observed and CE is just as good as a graphite anode. This phenomenon stresses that the CC/Li-clusters composite anode have outstanding electrochemical reversibility and high CE so that they could have a bright future for practical use. Moreover, the charge/discharge voltage profiles (Figure 4E) of the CC/LCO cell of different cycles look very different than those of the Li/LCO cell (Figure 4D).

Via the above work, we demonstrate that the controlled over-lithiation of carbon materials such as CC can effectively enhance the specific capacity without hurting the cycling performance. The key point is to obtain reversible and electrochemically active Li clusters, not Li dendrites. By making the carbon/Li clusters composite anode, we can significantly gain extra specific capacity and high CE, and eliminate the tedious and costly precycling and prelithiation procedure. This effective and facile approach greatly simplifies the process and provides

a new way to design high-capacity anode for next-generation high-energy-density LIBs.

In this work, we discover a new metastable form of Li, Li clusters, that forms between LiC_6 and Li dendrites during over-lithiation. The tiny Li clusters exhibit high transformation activity between Li^+ and Li, so the CE of the CC/Li clusters composite anode can reach 99.9% after the first several cycles, analogous to that of graphite anode. Furthermore, the CC/Li clusters composite anode owns high first-cycle CE and can be assembled into full cells without precycling or Prelithiation process. By utilizing bare CC as the anode and excessive $LiCoO_2$ as the cathode, respectively, to assemble the full cell, the Li clusters are observed on the carbon fiber. The CC/LCO full cell possesses high specific capacity and much better cyclic stability in 200 cycles than the Li/LCO cell. The controlled deposition of Li clusters and facile battery assembly are more feasible than the existing Li-metal-composite anode to practically enhance the energy density of the LIBs.

Experimental Section

Li Metal Deposition: Carbon cloth (WOS1009, Cetech Co., Ltd, 330 μm thick and 11.5 mg cm^{-2}) was chosen as the substrate to deposit Li metal. The half cells for Li metal deposition were assembled in 2025-type cell coins with carbon cloth as the working electrode, Li foil (500 μm, MTI Corporation) as the reference and counter electrode. A Celgard 2325 microporous membrane was used as the separator. The electrolyte was the 1 M LiTFSI (99.9%) in 1,3-dioxolane/1,2-dimethoxy-ethane (DOL/DME) (99.9%, v/v = 1:1) with 1% $LiNO_3$ (99.8%, Shanghai Xiaoneng Corp.). The battery assembly was completed in a glove box filled with Ar atmosphere (H_2O < 1 ppm, O_2 < 1 ppm) with 100 μL electrolyte each. The Li metal deposition was carried out on a LAND CT2001A cell tester.

Coulombic Efficiency Tests: Coulombic efficiency was measured with a galvanostatic discharge/charge process on a LAND CT2001A cell tester in a certain capacity range. The cells used the same configuration as described above. In a typical process, a low current density of 0.2 mA cm^{-2} was used in the first cycle to activate the electrode and form a stable SEI layer. After that, the carbon cloth was cycled at high current densities with different specific capacities. Besides, the stripping/plating tests for the CC/Li-metal composite anode were performed at a current density of 1 mA cm^{-2} with 1 mAh cm^{-2}.

Full Cell Tests: Bare carbon cloth and Li metal anodes were assembled with commercial $LiCoO_2$ cathode to fabricate full cells (denoted as Li/LCO and CC/LCO cells, respectively) for galvanostatic cycling tests. $LiCoO_2$ (LCO) electrodes were fabricated with a standard slurry process (provided by Shanghai Xiaoneng Tech.). LCO, super P (Timcal), and polyvinylidene fluoride (PVDF) (KYNAR HSV 900) were mixed in the weight ratio of 94:3:3 for slurry preparation. The slurry was spread on an Al foil with a loading mass of 18.9 mg cm^{-2} (about 3.0 mAh cm^{-2}). A Celgard 2325 microporous membrane was used as the separator. The electrolyte was the commercial 1.0 M $LiPF_6$ (99.9%) in a mixture of ethylene carbonate, dimethyl carbonate, and ethyl methyl carbonate (99.5%, volume ratio of 1:1:1, Shanshan Corp.). CR2025-type coin cells were assembled in an Ar-filled glovebox (H_2O < 1 ppm, O_2 < 1 ppm) with 100 μL electrolyte each. The electrochemical measurements were conducted at room temperature. The galvanostatic cycling test was carried out with A LAND CT2001A cell tester at a current density of 0.6 mAh cm^{-2} (about 0.2 C) in a voltage range of 4.3–2.7 V for Li/LCO and 4.3 to 2.5 V for CC/LCO, respectively.

Materials Characterization: The cycled electrodes were washed thoroughly with electrolytic solvent and dried at 70 °C in the glove-box for morphology characterization. SEM images were taken on a TESCAN Mira3 field emission scanning electron microscopy. Time-of-flight secondary ion mass spectrometry (TOF-SIMS) and TOF-SEM were carried out on a TESCAN Gaia3 FESEM. The sample was prebeamed to wipe off the influence of the SEI layer. XRD patterns were collected on a BRUKER D8 ADVANCE Da Vinci Poly-functional X-Ray Diffractometer (Cu Kα, λ = 1.54178 A). X-ray photoelectron spectroscopic (XPS) measurements were performed on a Kratos AXIS Ultra DLD spectrometer with a monochromatic Al Ka X-ray source. Raman spectra were recorded on a DXR Raman microscope (Senterra R200-L) with an excitation length of 532 nm.

Supporting Information

Supporting Information is available from the Wiley Online Library or from the author.

Conflict of Interest

The authors declare no conflict of interest.

[1] R. Schmuch, R. Wagner, G. Hörpel, T. Placke, M. Winter, *Nat. Energy* **2018**, *3*, 267.

[2] a) D. Lin, Y. Liu, Y. Cui, *Nat. Nanotechnol.* **2017**, *12*, 194; b) D. Lin, Y. Liu, A. Pei, Y. Cui, *Nano Res.* **2017**, *10*, 4003; c) A. Zhamu, G. Chen, C. Liu, D. Neff, Q. Fang, Z. Yu, W. Xiong, Y. Wang, X. Wang, B. Z. Jang, *Energy Environ. Sci.* **2012**, *5*, 5701.

[3] a) J. Qian, W. A. Henderson, W. Xu, P. Bhattacharya, M. Engelhard, O. Borodin, J.-G. Zhang, *Nat. Commun.* **2015**, *6*, 6362; b) W. Xu, J. Wang, F. Ding, X. Chen, E. Nasybulin, Y. Zhang, J.-G. Zhang, *Energy Environ. Sci.* **2014**, *7*, 513.

[4] D. Aurbach, E. Zinigrad, Y. Cohen, H. Teller, *Solid State Ionics* **2002**, *148*, 405.

[5] a) Y. Lu, Z. Tu, L. A. Archer, *Nat. Mater.* **2014**, *13*, 961; b) N. W. Li, Y. X. Yin, J. Y. Li, C. H. Zhang, Y. G. Guo, *Adv. Sci.* **2017**, *4*, 1600400.

[6] Y. M. Lee, J. E. Seo, Y.-G. Lee, S. H. Lee, K. Y. Cho, J.-K. Park, *Electrochem. Solid-State Lett.* **2007**, *10*, A216.

[7] a) B. Xu, W. Li, H. Duan, H. Wang, Y. Guo, H. Li, H. Liu, *J. Power Sources* **2017**, *354*, 68; b) X. Han, Y. Gong, K. Fu, X. He, G. T. Hitz, J. Dai, A. Pearse, B. Liu, H. Wang, G. Rubloff, Y. Mo, V. Thangadurai, E. D. Wachsman, L. Hu, *Nat. Mater.* **2016**, *16*, 572; c) Y. Li, B. Xu, H. Xu, H. Duan, X. Lü, S. Xin, W. Zhou, L. Xue, G. Fu, A. Manthiram, B. Goodenough John, *Angew. Chem., Int.*

Ed. **2017**, *56*, 753; d) L. Chen, Y. Li, S.-P. Li, L.-Z. Fan, C.-W. Nan, J. B. Goodenough, *Nano Energy* **2018**, *46*, 176.

[8] N. R. Brown, T. Makkapati, D. Teeters, *Solid State Ionics* **2016**, *288*, 207.

[9] A. C. Kozen, C.-F. Lin, O. Zhao, S. B. Lee, G. W. Rubloff, M. Noked, *Chem. Mater.* **2017**, *29*, 6298.

[10] a) X. Liang, Q. Pang, I. R. Kochetkov, M. S. Sempere, H. Huang, X. Sun, L. F. Nazar, *Nat. Energy* **2017**, *2*, 17119; b) S. S. Chi, Y. Liu, W. L. Song, L. Z. Fan, Q. Zhang, *Adv. Funct. Mater.* **2017**, *27*, 1700348.

[11] R. Zhang, X. B. Cheng, C. Z. Zhao, H. J. Peng, J. L. Shi, J. Q. Huang, J. Wang, F. Wei, Q. Zhang, *Adv. Mater.* **2016**, *28*, 2155.

[12] a) Y. Zhang, B. Liu, E. Hitz, W. Luo, Y. Yao, Y. Li, J. Dai, C. Chen, Y. Wang, C. Yang, H. Li, L. Hu, *Nano Res.* **2017**, *10*, 1356; b) Y. Wang, Y. Shen, Z. Du, X. Zhang, K. Wang, H. Zhang, T. Kang, F. Guo, C. Liu, X. Wu, W. Lu, L. Chen, *J. Mater. Chem. A* **2017**, *5*, 23434.

[13] T. Wang, R. Villegas Salvatierra, A. S. Jalilov, J. Tian, J. M. Tour, *ACS Nano* **2017**, *11*, 10761.

[14] a) Q. Li, S. Zhu, Y. Lu, *Adv. Funct. Mater.* **2017**, *27*, 1606422; b) S. H. Wang, Y. X. Yin, T. T. Zuo, W. Dong, J. Y. Li, J. L. Shi, C. H. Zhang, N. W. Li, C. J. Li, Y. G. Guo, *Adv. Mater.* **2017**, *29*, 1703729; c) K. Yan, B. Sun, P. Munroe, G. Wang, *Energy Storage Mater.* **2018**, *11*, 127.

[15] a) C. Jin, O. Sheng, Y. Lu, J. Luo, H. Yuan, W. Zhang, H. Huang, Y. Gan, Y. Xia, C. Liang, J. Zhang, X. Tao, *Nano Energy* **2018**, *45*, 203; b) C. Jin, O. Sheng, J. Luo, H. Yuan, C. Fang, W. Zhang, H. Huang, Y. Gan, Y. Xia, C. Liang, J. Zhang, X. Tao, *Nano Energy* **2017**, *37*, 177; c) T.-T. Zuo, Y.-X. Yin, S.-H. Wang, P.-F. Wang, X. Yang, J. Liu, C.-P. Yang, Y.-G. Guo, *Nano Lett.* **2018**, *18*, 297.

[16] R. Zhang, X. R. Chen, X. Chen, X. B. Cheng, X. Q. Zhang, C. Yan, Q. Zhang, *Angew. Chem., Int. Ed.* **2017**, *56*, 7764.

[17] J. Qian, D. Adams Brian, J. Zheng, W. Xu, A. Henderson Wesley, J. Wang, E. Bowden Mark, S. Xu, J. Hu, J. G. Zhang, *Adv. Funct. Mater.* **2016**, *26*, 7094.

[18] Y. Sun, G. Zheng, Z. W. Seh, N. Liu, S. Wang, J. Sun, H. R. Lee, Y. Cui, *Chem* **2016**, *1*, 287.

[19] S. Song, H. Yang, H. Su, Z. Jiang, Z. Lu, *Chem. Eng. J.* **2016**, *306*, 504.

[20] A. Funabiki, M. Inaba, T. Abe, Z. Ogumi, *J. Electrochem. Soc.* **1999**, *146*, 2443.

[21] J. R. Dahn, *Phys. Rev. B* **1991**, *44*, 9170.

[22] Y. Gogotsi, R. M. Penner, *ACS Nano* **2018**, *12*, 2081.

[23] D. Adams Brian, J. Zheng, X. Ren, W. Xu, J. G. Zhang, *Adv. Energy Mater.* **2018**, *8*, 1702097.

[24] Z. Lu, Z. Zhang, X. Chen, Q. Chen, F. Ren, M. Wang, S. Wu, Z. Peng, D. Wang, J. Ye, *Energy Storage Mater.* **2018**, *11*, 47.

[25] a) K. Yan, Z. Lu, H.-W. Lee, F. Xiong, P.-C. Hsu, Y. Li, J. Zhao, S. Chu, Y. Cui, *Nat. Energy* **2016**, *1*, 16010; b) K. Yan, H.-W. Lee, T. Gao, G. Zheng, H. Yao, H. Wang, Z. Lu, Y. Zhou, Z. Liang, Z. Liu, S. Chu, Y. Cui, *Nano Lett.* **2014**, *14*, 6016; c) K.-H. Chen, K. N. Wood, E. Kazyak, W. S. LePage, A. L. Davis, A. J. Sanchez, N. P. Dasgupta, *J. Mater. Chem. A* **2017**, *5*, 11671.